Finite Element and Experimental Analysis of Closure and Contact Bonding of Pores During Hot Rolling of Steel

SOO-HYUN JOO, JAIMYUN JUNG, MYUNG SIK CHUN, CHANG HO MOON, SUNGHAK LEE, and HYOUNG SEOP KIM

The closure and contact bonding behavior of internal pores in steel slabs during hot rolling was studied using experiments and the finite element method (FEM). Effects of pore size and shape were investigated, and three different cases of pore closure results were observed: no closure, partial closure, and full closure. The FEM results well reproduced various closure events. Bonding strengths of unsuccessfully closed pores, measured by tensile tests, showed critical effects. Also, there was a difference in bonding strengths of several fully closed pores. Fracture surfaces showed that welded regions could be divided into three (not, partially, and perfectly) welded regions. The pressure–time curves obtained from the FEM results indicate that pore surface contact time and deformed surface length are important parameters in pore welding. Pore size, pore shape, time of pressure contact, and deformed surface length should be considered to completely eliminate pores in final products.

DOI: 10.1007/s11661-014-2319-9

I. INTRODUCTION

THE inside, especially near the center, of materials produced *via* continuous casting or ingot casting retains numerous pores and defects. Porosity ranges in size from micro- to macro-pores. Macro porosity further ranges from millimeter- to centimeter-sized centerline shrinkage pores.[1–3] Pores inside a material pose adverse effects on mechanical properties such as strength and fatigue limit. Therefore, removal of such pores through post-casting processing is important for the quality improvement of the products. Micro-sized pores are extensively welded up, even by relatively small rolling reductions. On the other hand, the macro-sized pores are not easily welded up and can cause rapid failure when they remain in the final product. Therefore, the pore closure results from post-casting processing have been of great interest to many researchers.[4–8]

Although experiments with conditions identical to the actual processing are the most precise method for studying pore closure during post-casting processes, research based on such experiments is limited due to excessive cost, manpower, and equipment. Plasticine- or wax-based physical modeling was introduced as an alternative but was not able to offer accurate stress and strain data during processing.[9–11] Thus, there has been an increasing interest in investigating the details of closure of internal pores during the post-casting process using computer simulations. Theoretical simulations are not only capable of reproducing actual conditions of the experiments but also capable of predicting load, flow of metals, stress distribution, and strain distribution. The FEM, among various simulation tools, has been one of the most popular simulation methods used for understanding the deformation behavior and closure events of the internal pores, because it is able to analyze materials with complicated shapes.[12–19]

Residual pores that remain after casting are generally removed by applying compressive stress or by heating. In this study, hot rolling was employed for removing pores. Removing pores is a two-step process.[20] The first step is the densification of pores using rolling to remove the overall configuration of the pores. Then, during the second step, complete removal is achieved by welding between the pore surfaces using thermal energy (hot rolling). If densification is insufficient during the first step, the pore edges tend to become sharp and can easily become crack initiation sites. Moreover, if complete welding is not attained during the second step, then the bonding strength is significantly less than the tensile strength of the material. This causes the product to be prone to crack propagation during deformation due to separation at the pores before the tensile strength of the material in sound regions is exceeded. Therefore, it is necessary to conduct research based on comprehensive understanding, analysis, and experimentation with optimal conditions for pore closure and welding under various hot rolling conditions.

Analysis of the densification behavior of pores can be achieved using the mechanical properties of that

SOO-HYUN JOO and JAIMYUN JUNG, Ph.D. Candidates, are with the Department of Materials Science and Engineering, Pohang University of Science and Technology, Pohang 790-784, Republic of Korea. MYUNG SIK CHUN, Senior Principal Researcher, and CHANG HO MOON, Principal Researcher, are with the Technical Research Laboratories, POSCO, Pohang 790-785, Republic of Korea. SUNGHAK LEE and HYOUNG SEOP KIM, Professors, are with the Department of Materials Science and Engineering, Pohang University of Science and Technology, and also with the Center for Aerospace Materials, Pohang University of Science and Technology, Pohang 790-784, Republic of Korea. Contact e-mail: hskim@postech.ac.kr

Manuscript submitted October 15, 2013.
Article published online May 1, 2014

Table I. Chemical Composition of Low-Carbon Steel

C (Pct)	Si (Pct)	Mn (Pct)	P (Pct)	S (Pct)
0.180 to 0.230	0.150 to 0.350	0.300 to 0.600	0.030	0.035

material in the FEM, but the analysis for welding behavior demands experimentally measured bonding strengths of the welded surfaces. Chaaban and Alexander[21] led research on closure behavior of pores under hot forging through billets with drilled-in cylindrical pores. They indicated that despite clear internal contact of the pore surfaces, no clear welding was established. Under an optical microscope (OM), they observed a distinct separation of the pore surface. They proposed that pore welding was established when the billet's surface area decreased by 60 pct. Afterward, by observing that material fractures first occurred at the surface of the welded pore during a bending test, Chaaban and Alexander concluded that even after complete densification, pores were still fatal. The lower bonding strengths of the welded surfaces of pores degraded the mechanical properties of the processed materials.[22–24] Thus, because low bonding strength may lead to cracks at the bonding sites, research to understand densification of pores and predict bonding strength is necessary.[25,26] Compared to research results on pore closure behavior under free forging,[9–14,25–28] results based on the rolling process[10,15,29–31] are scarce. Moreover, there has been only a handful of published works despite a clear need for research comparing experimental and FEM analyses.

In this research, experimental results were compared with FEM results and used to analyze the densification behavior of pores and bonding strength after rolling. There was also an extensive investigation on how conditions such as pore size and shape affect closure and contact bonding of pores. The validity of FEM analysis was confirmed by actual experimental results. The FEM analysis successfully predicted the densification behavior of the pores, which is the first step in pore closure behavior. Afterward, pore bonding strength was measured through tensile tests, and FEM analysis proved to be effective in understanding the optimal conditions for pore welding behavior.

II. EXPERIMENTAL AND FEM ANALYSES

The material used for rolling tests was conventional carbon steel (KS:SM20C) with 0.18 to 0.32 pct carbon content. The composition of the experimental material is indicated in Table I. The specimen geometry was 300 mm in length, 50 mm in width, and 16 mm in thickness. To observe the densification and closure behavior of pores, cylindrical pores with radii of 1, 2, and 4 mm were placed transverse to the length direction of the specimen. In order to examine the pore shape effect, 1-mm circular pores and elliptical pores with major and minor axes of 2 and 0.5 mm, respectively, were constructed. The elliptical pores rolled in the rolling direction (RD elliptical pores) and the elliptical pores rolled in the normal direction (ND elliptical pores) were distinguished as shown in Figure 1. The shrinkage of a pore may affect the responses of neighboring pores. From prior FEM simulations, the affected regions due to existing pores were defined by altered stress field. Each preceding pore was positioned from the next pore by a distance proportional to the preceding pores size. The properly designed distances of the neighboring pores eliminated multiple pores effect.

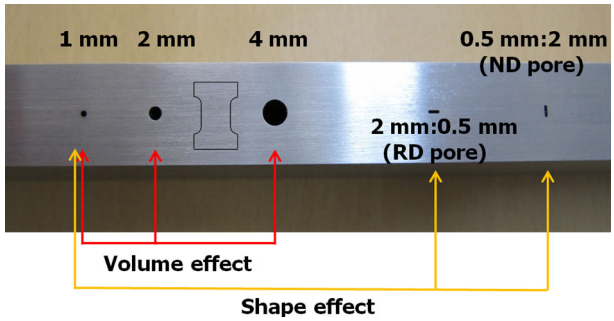

Fig. 1—Precisely machined pores in rolling specimens and the sketch of tensile samples.

The rolling test was designed to have a roll die of 300-mm diameter, same top–bottom roll speed (1.57 m/s), and thickness reduction ratios of 11.2 and 31.3 pct. The specimen was pre-heat treated at 1273.15 K (1000 °C) for 25 minutes before rolling. The surface temperature of the specimen was measured using an infrared camera before and after rolling. The specimen was quickly water-cooled after the rolling process.

Densification was measured by OM to compare the actual experiment and the plane-strain conditions based on two-dimensional FEM simulations. Tensile tests were performed on the specimens after pore densification in order to measure the bonding strength of the welded pore surfaces. After observing the position of each pore, a tensile specimen was machined with the welded surface of the pore at the center of the specimen. The overall length was designed as 9 mm due to thickness of rolled materials, and width of grip section was 6 mm. The final specimen was 2 mm in gage length, 4 mm in width, and 2 mm in thickness. The sketch of tensile samples is exhibited in Figure 1 between 2-mm and 4-mm pores. A universal testing machine (RB model 301 UNITECH M, R&B Co., Korea) was used for tensile testing, and the strain rate was 1×10^{-3} s^{-1} for all specimens. Four tensile tests for each condition were performed in order to obtain reliable bonding strengths. After the tensile test, fracture surfaces were observed using field emission scanning electron microscope (FE-SEM, JSM 6330F, Jeol, Japan).

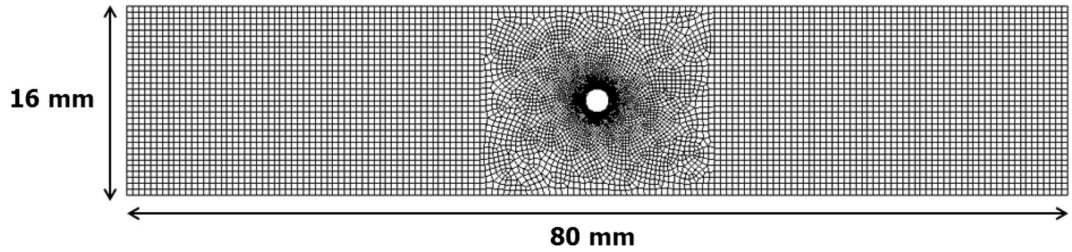

Fig. 2—Dimension and initial mesh of a rolling specimen with a 2-mm pore.

For the FEM analysis, the popular FEM package for elastic–plastic material deformation (ABAQUS V6.8, Simulia Co., USA) was utilized under the 2D plane-strain condition. The dynamic explicit FEM code was used to accurately simulate the rolling process. The measured temperatures of the rolling materials before and after the process showed small differences [less than 30 K (30 °C)]. Therefore, thermo-mechanical coupling was not considered in order to reduce computational time. To perfectly simulate the experimental condition of many pores, a vast amount of mesh is required, which comes at a computational cost, leading to inefficiency. Therefore, while sustaining a reasonable specimen length of 80 mm, a single pore was set as shown in Figure 2. Nodes unaffected by the pore were separated by 0.5 mm, and 80 to 100 nodes were set on the pore surface. This made the mesh fine enough for a detailed examination of the densification behavior. The mesh type was set as a combination of CPE4R and CPE2, and the overall mesh number was set at 10,000 to effectively reduce the computational time. The roll die was set as a rigid body and the specimen as elastic–plastic deformable. The contact frictional coefficient was set at 0.35, which falls into a typical range for hot-rolling processes. Shida's constitutive equation[32] was employed for the flow stress of the material. Shida's constitutive equation is valid under the conditions of carbon content in a range of 0.07-1.2 pct, a temperature range of 973.15 K to 1473.15 K (700 °C to 1200 °C), strain near 0.7, and a strain rate of approximately 100 s^{-1}. These conditions, required for Shida's constitutive equation, matched well with the experimental conditions of this research, which were 0.2 pct carbon content, and 1223.15 K (950 °C) before and after the rolling process. Shida's equation was thus used to determine the flow stress of the material, which was necessary for the FEM analyses. Both elasticity and plasticity were assumed to be isotropic with a Poisson's ratio of 0.3.

III. COMPARATIVE ANALYSIS BETWEEN EXPERIMENTAL AND FEM RESULTS

A. *Comparative Analysis of Rolled Pore Shape*

After the rolling process, the specimen was examined using OM to determine the degree of densification. The unclosed pores were easily observable when pore surfaces were not in contact and welding did not occur. However, because clear distinctions between fully closed and partially closed pores were tough to observe without prior treatment, 2 pct Nital etchant was used for surface etching to get a clear picture of welded pore surfaces (Figure 3).

In the case of the initial 1-mm circular pores, 10 pct rolling did not caused noticeable densification (Figure 3(a)), so they were categorized as unclosed. However, 30 pct reduction rolling led to a completely welded pore surface (Figure 3(a)) and was categorized as fully closed. The initially 2-mm circular pores, subjected to both 10 and 30 pct reduction rolling, exhibited behavior identical with the 1-mm circular pores (Figure 3(b)). The initially 4-mm circular pores were not closed after 10 pct reduction rolling due to scarce densification near the center of the pore, but were partially closed after 30 pct reduction rolling.

In the case of the RD elliptical pores, both 10 and 30 pct reduction rolling induced complete densification, but detailed examination under an OM indicated that densification after 10 pct reduction rolling left two edge regions of the pore slightly open (Figure 3(d), yellow circle). In the case of the ND elliptical pores rolled normal to the major axis, the pores were unclosed after 10 pct reduction rolling, but fully closed after 30 pct reduction. While closure was observed for all other types of pores in the direction of the specimen thickness, ND elliptical pores showed densification only after 30 pct reduction rolling. Also, similar to results for the RD elliptical pores, the ND elliptical pores went through insufficient densification at the two ends of the pore (Figure 3(e), yellow circle). Because the ND elliptical pores, after the rolling process, showed full densification in the direction of the roll, the tensile specimen was processed so that the direction of the tension coincided with the rolling direction.

Qualitative analysis of both FEM and experimental results under three classifications (unclosed, partially closed, and fully closed) showed that both results were identical (Figure 3). Notably, both the FEM and experimental results on the 4-mm pores with 30 pct reduction rolling showed no densification, RD elliptical pores with 10 pct rolling showed full densification while not complete on the end regions, and ND elliptical pores with 30 pct rolling showed full densification in the rolling direction while not completely on the end regions. These were all in complete agreement, thus confirming the accuracy of FEM prediction.

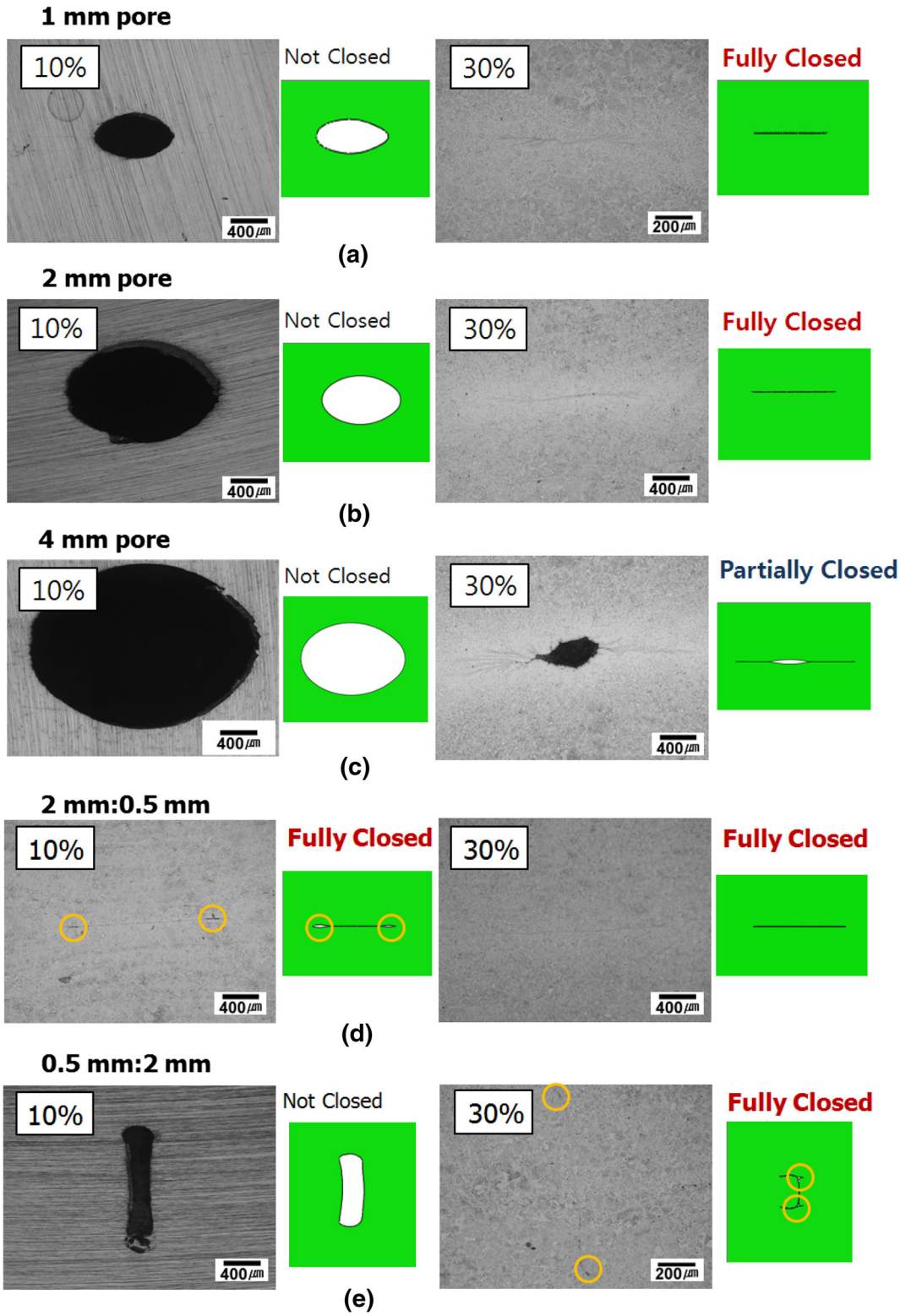

Fig. 3—Comparison of deformed pores in experimental and FEM results: (*a*) 1-mm pore, (*b*) 2-mm pore, (*c*) 4-mm pore, (*d*) RD pore, and (*e*) ND pore (Color figure online).

B. *Tensile Test Results*

The bonding strengths of the five fully closed pores after the rolling tests (30 pct rolling of 1-mm pore, 30 pct rolling of 2-mm pore, 10 pct rolling of RD pore, 30 pct rolling of RD pore, and 30 pct rolling of the ND pore) in Figure 3 cannot be identical. In order to

Table II. Tensile Strength of Matrix and Bonding Strength of Pores

	Tensile Strength (MPa)
Matrix, 10 pct reduction	601.9 ± 6.5
Matrix, 30 pct reduction	608.5 ± 4.5
Pore shape and reduction	bonding strength
4 mm, 30 pct reduction	47.8 ± 21.4
2 mm, 30 pct reduction	330.4 ± 53.2
2 mm: 0.5 mm, 10 pct reduction	369.5 ± 32.5
1 mm, 30 pct reduction	563.1 ± 4.0
2 mm: 0.5 mm, 30 pct reduction	586.8 ± 7.9
0.5 mm: 2 mm, 30 pct reduction	589.4 ± 4.1

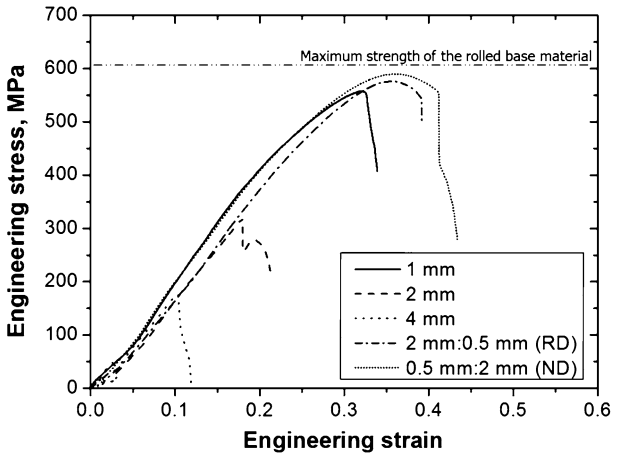

Fig. 4—Engineering stress–strain curves of 30 pct rolled pore samples.

evaluate the bonding strength of the each closed pore, tensile specimens were made with welded surfaces at the center. To compare the bonding strength to the strength of a pore-free matrix, the specimens were made so that the tensile direction of the transverse direction (TD) surface of the pore-free regions coincided with the thickness direction of the rolled specimen. The matrix of the 10 pct rolled specimen showed a tensile strength of 601.9 MPa while that of the 30 pct rolled specimen was 608.5 MPa (Table II).

In the tensile test results in Figure 4, welded surface strength, or bonding strength, was divided into three cases. First is the case of partially closed pores. Tensile tests on the specimen with partially closed pores, after 30 pct rolling of the 4-mm pore sample, showed that the bonding strength of the partially closed region was only 47.8 MPa. The overall tensile strength of the specimen was 177.8 MPa, confirming that pores that did not undergo full densification, significantly weakened the mechanical properties of the material. The second case was when the bonding strength was low despite fully closed pores. The bonding strength of the fully closed pores after 30 pct rolling of the 2-mm pore sample was 330.4 MPa. After the separation of the welded surface caused an immediate decrease in load, work hardening of the matrix was perceived, and finally fracture occurred. The third case was when the bonding strength of fully closed pores was similar to the tensile strength of a pore-free specimen. The bonding strength of a fully closed pore after 30 pct rolling of the 1-mm pore sample was 563.1 MPa, which was just a little less than the tensile strength of the matrix. No sudden decrease in load due to separation of the welded surface was observed, and the tensile specimen experienced necking. The tensile test demonstrated that partially closed pores were more fatal to the mechanical properties of a material than were fully closed ones. Also, there was disparity between bonding strengths of several fully closed pores.

Even though every pore was fully closed, there were clear differences in bonding strengths. In fact, the bonding strengths of the 1-mm circular and two elliptical pore samples were all above 550 MPa, but the bonding strength of the 2-mm circular pore sample was 324 MPa. These were clear differences despite that they were all fully closed. This result indicates that because a pore size affects its densification behavior, it also affects the bonding strength after densification.

The tensile test also showed that the shape of a pore also affects its bonding strength of the pore. Under 30 pct reduction rolling, the RD elliptical pores were better bonded than 1-mm pores. Also, the RD elliptical pores were fully closed after 10 pct rolling, but ND elliptical pores were not. Nevertheless, both types of pores were fully closed with the strongest bonding strength (589 MPa) after 30 pct rolling. This result shows that the bonding strength of a closed pore is highly dependent on the shape and direction of the pore.

C. *Tensile-Fractured Surface*

After the tensile tests, analysis on the fracture surface of each specimen was conducted. The fracture surface of a specimen with partially closed pores after 30 pct rolling of 4-mm pore could be divided into two regions (Figure 5(a)). There was a central region where the pore was not closed, and a region where the pore was partially closed. The unclosed region could be distinguished by flat fracture surfaces (Figure 5(b)). The partially closed region could be recognized by a partially welded region, or a region with a combination of dimpled and flat fracture surfaces (Figure 5(c)). In comparison, the fracture surface of the sample without pore showed the ductile fracture mode with dimples and some inclusions without any flat area (Figure 5(d)).

The fracture surfaces of specimens with 10 and 30 pct rolled RD elliptical pore samples are presented in Figure 6. The fracture surface of the 10 pct rolled specimen (Figure 6(a)) showed uniform distribution of the partially welded regions. However, as predicted in the FEM analysis, the two ends of the pore did not exhibit any densification behavior, and thus, the unwelded regions were observed both on each end. The fracture surface of the 30 pct rolled specimen showed well-distributed welded regions (Figure 6(c)) and perfectly welded region (Figure 6(d)). The tensile test results showed that the 10 pct rolled specimen exhibited approximately 50 pct of the bonding strength of a pore-free specimen, indicating that increasing the

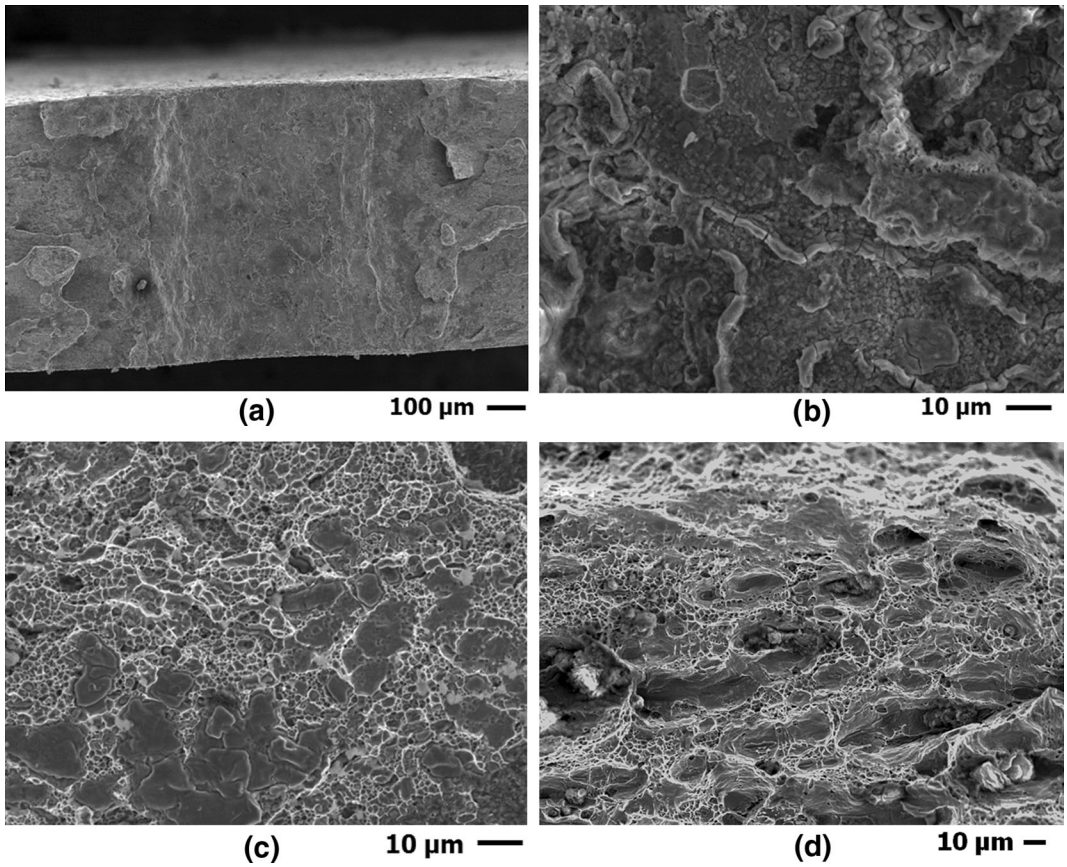

Fig. 5—(*a*) Fracture surface after a tensile test of a 30 pct rolled 4-mm pore sample: (*b*) unclosed region: (*c*) locally welded region: (*d*) tensile test on sample without pore.

extent of partially welded regions significantly decreases the mechanical properties of a material.

The fracture surfaces of specimens with 30 pct rolled 1 and 2-mm circular pores revealed that the specimen with 2-mm circular pores had a larger unwelded region near the center than the specimen with 1-mm circular pores did (Figures 7(a) and 7(b)). The 30 pct rolled 2-mm circular pore sample had a low bonding strength of 330 MPa. This could be because the partially welded region could act as a crack initiation site that lowers the strength of the entire specimen. From a microscopic point of view, the 30 pct rolled specimen with 2-mm pores contained an unwelded region near the center (Figure 7(c)), while perfectly welded in other areas (Figure 7(d)).

D. *Pressure–Time Curves*

FEM simulations were conducted to pinpoint the factors affecting the bonding strength of welded surfaces of fully closed pores. Because hydrostatic pressure is well known to be the prominent factor that affects the densification of pores, pressure–time curves were employed to explore the hydrostatic pressure that acts on the welded surface of a pore during densification.

The FEM results on a 30 pct rolled 1-mm pore sample were the first to be investigated (Figure 8). The applied pressure was taken as an average value from the contact region of the pore surface. The densification was initiated near the two edges of the pore (Figure 8(b)), and the pressure at the moment was high due to the shape effect. Afterward, at the time of complete densification (Figure 8(d)), the shape effect was undetected and the pressure on pore surface and on the matrix became continuous. Because the densification near the center of a pore usually happens last, and because the tensile test result confirmed that pore closure at the center considerably affects the mechanical properties, the peak pressure on the center of a fully closed pore was of key interest in the analysis.

In Figure 9 the pressure–time curves from FEM on fully closed pores after 30 pct rolling confirmed that the maximum pressure values of fully closed pores were similar. However, a big difference in the amount of time the pressure acts on a welded pore surface was observed. In FEM simulation results on 30 pct rolling, compressive hydrostatic pressure was observed at the position indicated by a black arrow in Figure 8(b) when a pore was fully closed. Before a full closure, tensile hydrostatic pressure was applied. Therefore, the applied hydrostatic pressure and time are strongly related with how soon a pore is collapsed and closed. In the FEM results, pore closures for 1-mm, 2-mm, and RD pores were achieved before reaching maximum pressure region, so, the applied maximum pressures ended up almost the same. The RD pore showed the fastest closing behavior, and

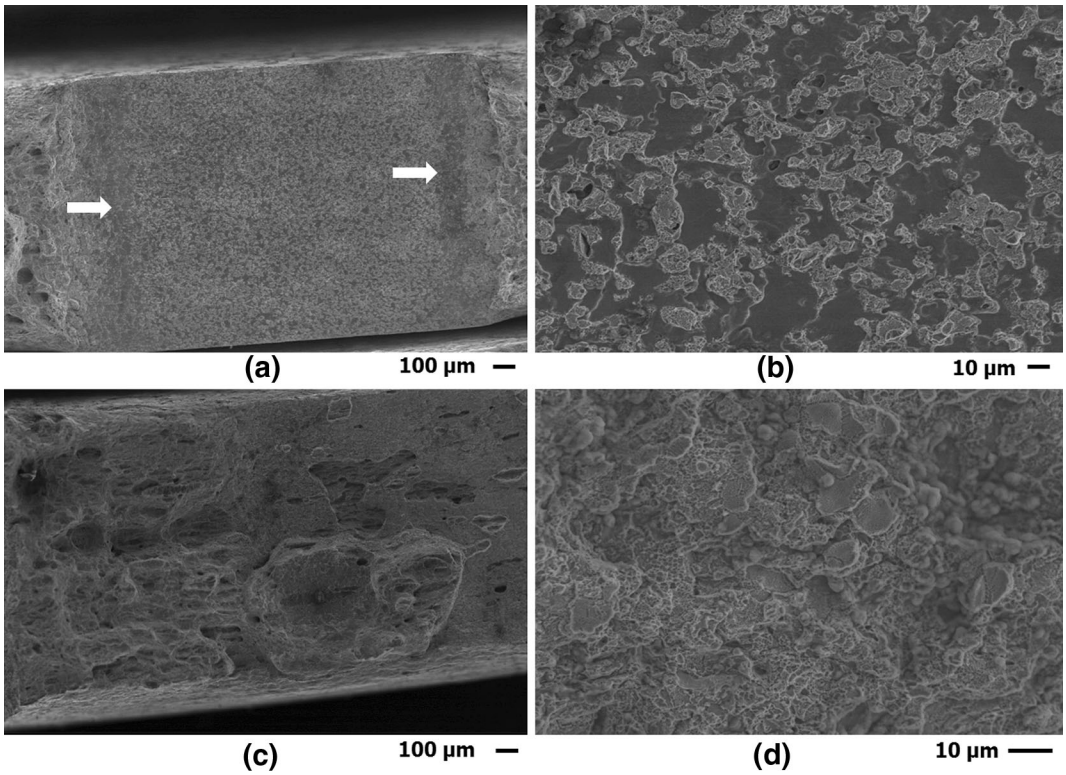

Fig. 6—(*a*) 10 pct rolled RD pore sample surface after a tensile test, (*b*) locally welded 10 pct rolled RD pore sample surface, (*c*) 30 pct rolled RD pore sample surface after a tensile test, and (*d*) 30 pct rolled perfectly welded RD pore sample surface.

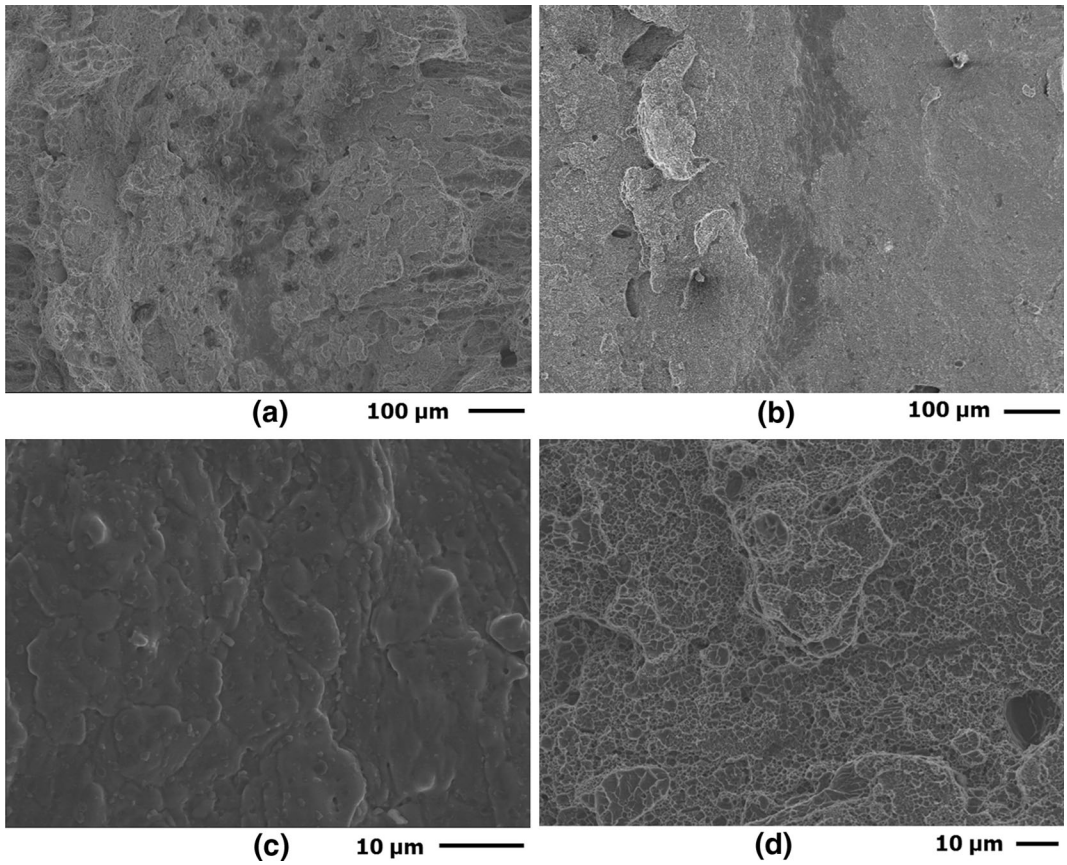

Fig. 7—(*a*) 30 pct rolled 1-mm pore sample surface after a tensile test, (*b*) 30 pct rolled 2-mm pore sample surface after a tensile test, (*c*) unwelded region in 30 pct rolled 2-mm pore sample, and (*d*) perfectly welded region in 30 pct rolled 2-mm pore sample.

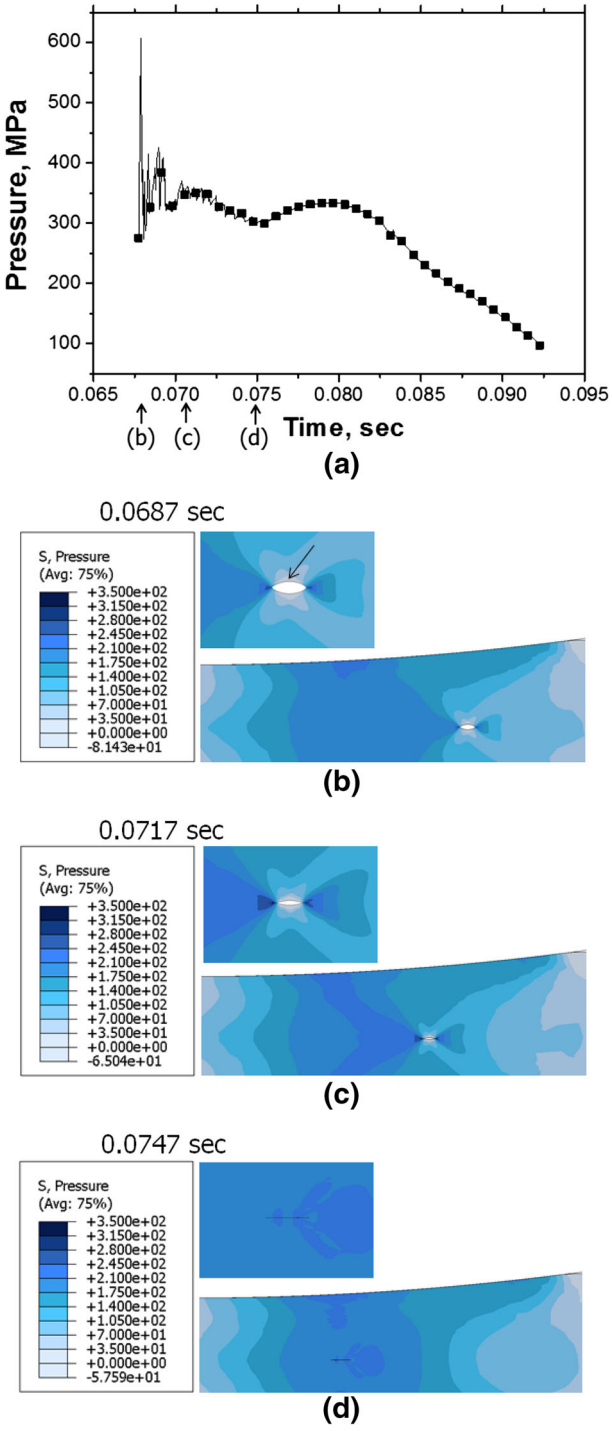

Fig. 8—(*a*) Pressure–time curve obtained from 1 mm 30 pct rolled pore FEM result test, (*b*) Pressure distribution at 0.0687 s, (*c*) Pressure distribution at 0.0717 s, and (*d*) Pressure distribution at 0.0747 s.

closure of the 1-mm pore happened earlier than that of 2-mm pore. Therefore, the 1-mm pore underwent longer time with a pressure of around 300 MPa than the 2-mm pore did. The surface of the 2-mm circular pore had the shortest time span and the tensile test showed its bonding strength to be 330.4 MPa. In contrast, the RD elliptical pores, which had the longest time span,

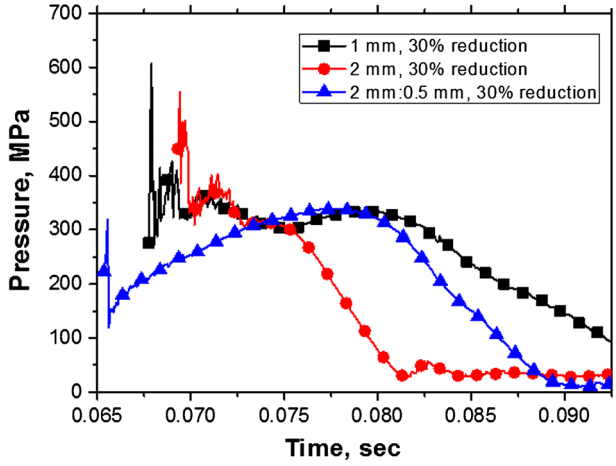

Fig. 9—Pressure–time curve obtained from 1 mm 30 pct, 2 mm 30 pct, and RD 30 pct pores.

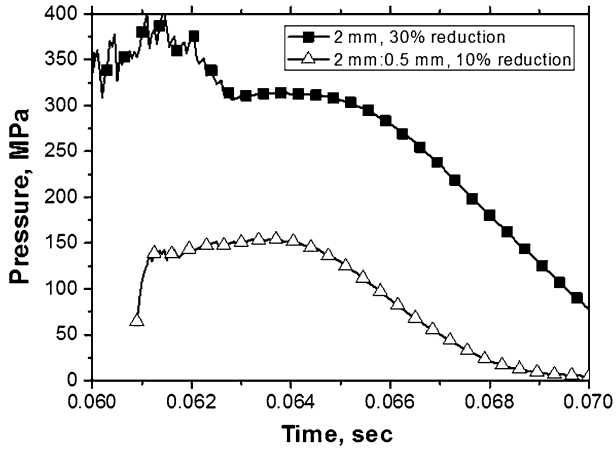

Fig. 10—Pressure–time curve obtained from 2 mm 30 pct and RD 10 pct pores.

had bonding strengths of 586.8 MPa. The result shows that the welding between pore surfaces is diffusion controlled, and thus it is confirmed that the amount of time the pressure acts on the surface is a vital factor.

The most peculiar pressure–time curve analysis result was observed while comparing the pressure–time curves of the 30 pct rolled 2-mm circular pore sample and the 10 pct rolled RD elliptical pore sample. The pressure–time curve analysis results from the FEM (Figure 10) showed that the maximum pressure was approximately 300 MPa for the circular pores, while only 150 MPa for the elliptical ones. It was also found that the time that the pressure acted on a pore was longest for the 2 mm pore sample. In order to seek out the reason behind this result, analysis on the length of the initial pore surface and the length of the pore surface after rolling was conducted (Table III). The lengths of the initial pores were 6.28 and 4.57 mm for the 2-mm circular and RD pore samples, respectively, and the lengths of the surfaces after rolling were 2.01 and 2.05 mm, respectively, based on OM images. The percent contraction for

Table III. Tensile Strength and Reduction Ratio Values of 2 mm Pore Sample After 30 Pct Rolling and RD Pore Sample After 10 Pct Rolling

	Bonding Strength (MPa)	Initial Surface Length (mm)	Deformed Surface Length (mm)	Reduction Ratio (Pct)
2 mm, 30 pct reduction	330.4 ± 53.2	6.28	2.01	313
2 mm: 0.5 mm, 10 pct reduction	369.5 ± 32.5	4.57	2.05	223

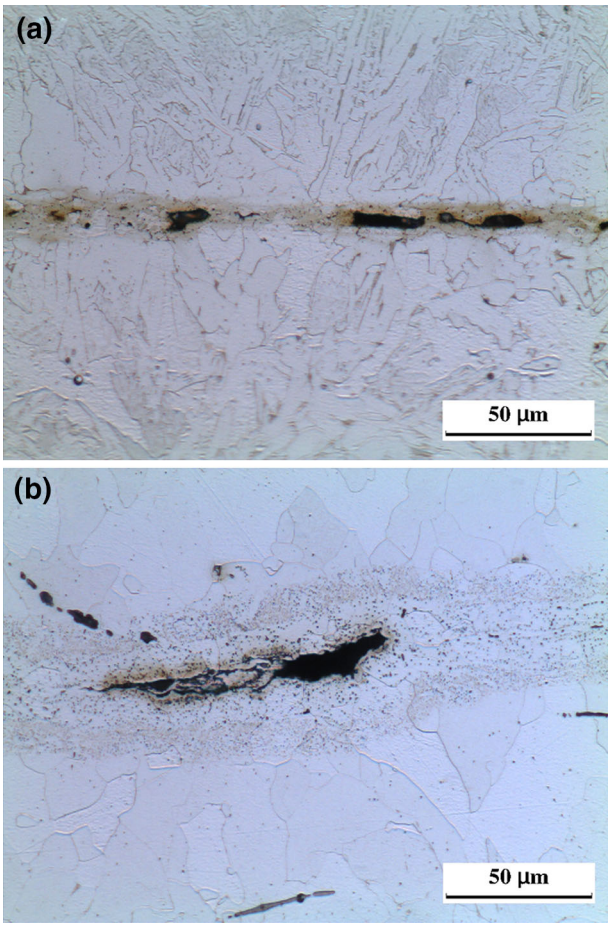

Fig. 11—Damaged zone with residual holes around a pore trace: (*a*) 10 pct rolled RD pore and (*b*) 30 pct rolled 2 mm pore.

the circular 2 mm pore was 313 pct while only 223 pct for the RD elliptical pore. Based on the results of the tensile fractured surface, the 2 mm pore sample consisted of an unwelded region at the center while perfectly welded on other regions (Figure 7). The fracture surfaces of the specimen with RD elliptical pores were partially welded overall (Figure 6).

The bonding regions were carefully observed using OM at higher magnification in Figure 11. There were damaged zones with a small size of residual holes around a pore trace. The 30 pct rolled 2-mm circular pore had larger damaged zone and larger sizes of the residual holes compared to these of 10 pct rolled RD elliptical pore. The widths of the damaged zone of the 10 pct rolled RD pore and the 30 pct rolled 2 mm pore were 10.5 and 43.5 μm, respectively. Recently, the process of crack healing in low-carbon steels under hot plastic deformation was investigated.[33] In their results, the density of residual holes around the preset crack zone decreased when the protrusions on the crack surfaces deformed easily. When larger contraction occurs on a pore during rolling, the contact surface decreases and the protrusions leave more holes. Porosity generally occurs as a result of gases dissolved in the melt, and then the pore surface is contaminated by gases. The impurity atoms from gases disturb surface welding. The 2 mm pore had larger initial surface length, but similar deformed surface length. This means that the 30 pct rolled 2 mm pore had relatively high density of surface impurity atoms. The matrix atoms within the specimen diffused toward the welded surface for a strong bond, but in the case of a large reduction ratio of a pore during rolling, the large density of impurity atoms at the pore surface impede the bonding process. Therefore, the 30 pct rolled 2 mm pore sample showed an unwelded region at the center and larger damaged zone. The small unwelded region caused by a large reduction ratio can be more harmful than overall partially welded pore can.

IV. CONCLUSIONS

To simulate the closure of pores in a cast material, comparative analyses based on experimental and FEM results from rolled 1, 2, and 4-mm circular pores, and RD and ND elliptical pores parallel to the TD direction of the product specimen, were conducted. The effect of pore shape on the overall densification behavior of pores was discovered by comparing the densification results of 1-mm circular pores and RD elliptical pores of the same size. The 1-mm circular pore surface was not welded under 10 pct reduction rolling, but the RD elliptical pores were fully closed except at the two ends of the major axis after 10 pct reduction rolling. Hence, it was concluded that pore shape significantly affects the densification behavior of pores, and that densification of pores can be effectively achieved by controlling the shapes and directions of pores before rolling.

The tensile fractured surface analysis confirmed that specimens with unclosed pores or partially welded regions experienced a substantial decrease in the bonding strength of the welded pores. In the case where pores were not fully closed (30 pct rolling of 4-mm circular pore sample), the tensile curve showed a sudden decrease in stress at the partially welded region, and the ultimate tensile stress of the specimen was considerably lower than that of the matrix material. After 10 pct rolling of the RD elliptical pore sample, the partially welded regions were well distributed, and a

significant decrease in the bonding strength of the welded pores was observed. Therefore, not only the densification behavior of pores, but also the pore surface bonding strength should be considered in any related research.

After 30 pct rolling, the elliptical pores had higher bonding strengths compared to the circular pores. The pressure–time curve for each type of pore showed that the pressure on each type was similar, but the amount of time the pressure acts was different for each type of pore, which resulted in different closing strengths. This result verifies that not only the maximum pressure due to the reduction ratio, but also the time that the pressure acts on pores is essential to the welding results. This is because the welding of pores is a diffusion controlled phenomena. Also, in the case of circular pores, the center regions were not welded, with some disparity in the size of the unwelded regions, depending on the reduction ratio. While both FEM and OM results confirmed that 2-mm circular pore after 30 pct rolling was fully closed, the closure surface at the center consisted of an unwelded region. The percentage of contraction for 2 mm pores showed a sizable 313 pct, with particularly significant contraction in the center region. It is speculated that the substantial contraction of the center region caused impurity atoms at the pore surface to disturb the welding process.

In this study, the bonding strength of the RD pore showed the highest value which is 96.5 pct of the strength of solid matrix. Not closed pores are fatal and fully closed pores can possess low bonding strength. From the experimental and FEM results of different pores, some conditions are generalized as conclusions to reach matrix strength. The pore welding behavior was different depending on the pore reduction ratio, time of pressure, and the magnitude of the pressure on the surface. Different combinations resulted in different bonding strengths. The higher magnitude and longer applied time of the pressure on the surface are beneficial. However, the large contraction of a pore produces small sizes of residual holes around a pore causing backwash bonding. Therefore, to fully control pore closure and welding, pore shape, time of pressure acting on the pore, and contraction of the pore should be comprehensively considered before rolling.

ACKNOWLEDGMENTS

This work was supported by POSCO. The simulation was supported by Grant No. KSC-2012-C2-09 from Korea Institute of Science and Technology Information.

REFERENCES

1. L. Leduc, T. Nadarajah, and C.M. Sellars: *Met. Technol.*, 1980, vol. 7, pp. 269–73.
2. L. Jia, D. Xu, M. Li, J. Guo, and H. Fu: *Met. Mater. Int.*, 2012, vol. 18, pp. 55–62.
3. B.-H. Son, J.-G. Hong, Y.-T. Hyun, S.-C. Bae, and S.-E. Kim: *Korean J. Met. Mater.*, 2012, vol. 50, pp. 100–06.
4. Y. Nadot, J. Mendez, N. Ranganathan, and S. Beranger: *Fatigue Fract. Eng. Mater. Struct.*, 1999, vol. 22, pp. 289–300.
5. P. Haušild, C. Berdin, P. Bompard, and N. Verdière: *Int. J. Press. Vessels Pip.*, 2001, vol. 78, pp. 607–16.
6. Y. Nadot, J. Mendez, and N. Ranganathan: *Int. J. Fatigue*, 2004, vol. 26, pp. 311–19.
7. Y. Uematsu, T. Kakiuchi, K. Tokaji, K. Nishigaki, and M. Ogasawara: *Mater. Sci. Eng. A*, 2013, vol. 561, pp. 386–93.
8. J.-J. Park: *Met. Mater. Int.*, 2013, vol. 19, pp. 259–70.
9. E. Erman, N.M. Medei, A.R. Roesch, and D.C. Shah: *J. Mech. Work. Technol.*, 1989, vol. 19, pp. 165–94.
10. M. Nakasaki, I. Takasu, and H. Utsunomiya: *J. Mater. Process. Technol.*, 2006, vol. 177, pp. 521–24.
11. Y.D. Kim, J.R. Cho, and W.B. Bae: *J. Mater. Process. Technol.*, 2011, vol. 211, pp. 1005–13.
12. Y.S. Lee, S.U. Lee, C.J. Van Tyne, B.D. Joo, and Y.H. Moon: *J. Mater. Process. Technol.*, 2011, vol. 211, pp. 1136–45.
13. G. Banazek and A. Stefanik: *J. Mater. Process. Technol.*, 2006, vol. 177, pp. 238–42.
14. X.-X. Zhang, Z.-S. Cui, W. Chen, and Y. Li: *J. Mater. Process. Technol.*, 2009, vol. 209, pp. 1950–59.
15. W. Deng, D.-W. Zhao, X.-M. Qin, L.-X. Du, X.-H. Gao, and G.-D. Wang: *Comp. Mater. Sci.*, 2009, vol. 42, pp. 439–47.
16. M.C. Lee, S.M. Jang, J.H. Cho, and M.S. Joun: *Int. J. Mod. Phys. B*, 2008, vol. 22, pp. 5768–73.
17. C.H. Jeon, S.W. Han, B.D. Joo, C.J. Van Tyne, and Y.H. Moon: *Met. Mater. Int.*, 2013, vol. 19, pp. 1069–76.
18. E.-Y. Kim, J.-H. Cho, H.-W. Kim, and S.-H. Choi: *Korean J. Met. Mater.*, 2013, vol. 51, pp. 41–50.
19. M. Rezayat and A. Akbarzadeh: *Met. Mater. Int.*, 2012, vol. 18, pp. 827–32.
20. A. Wang, P.F. Thomson, and P.D. Hodgson: *J. Mater. Process. Technol.*, 1996, vol. 60, pp. 95–102.
21. M.A. Chaaban and J.M. Alexander: *Proc. Mach. Tool Des. Res. Conf. 17th*, vol. 3, 1976, pp. 633–45.
22. K. Min, K. Kim, S.K. Kim, and D.-J. Lee: *Met. Mater. Int.*, 2012, vol. 18, pp. 341–49.
23. J.-S. Kim, K.S. Lee, Y.-N. Kwon, Y.-S. Lee, S. Lee, and Y.W. Chang: *Korean J. Met. Mater.*, 2013, vol. 51, pp. 547–57.
24. S. Lee, J.-S. Lee, Y.-B. Kim, G.-A. Lee, S.-P. Lee, I.-S. Son, J.-K. Lee, and D.-S. Bae: *Korean J Met. Mater.*, 2013, vol. 51, pp. 655–64.
25. C.Y. Park and D.Y. Yang: *J. Mater. Process. Technol.*, 1996, vol. 57, pp. 129–40.
26. C.Y. Park and D.Y. Yang: *J. Mater. Process. Technol.*, 1997, vol. 72, pp. 32–41.
27. K. Chen, Y. Yang, G. Shao, and K. Liu: *Comput. Mater. Sci.*, 2012, vol. 51, pp. 72–77.
28. H. Kakimoto, T. Arikawa, Y. Takahashi, T. Tanaka, and Y. Imaida: *J. Mater. Process. Technol.*, 2010, vol. 210, pp. 415–22.
29. A. Sjöström: *J. Mech. Work. Technol.*, 1982, vol. 6, pp. 347–60.
30. A. Chaijaruwanich, R.J. Dashwood, P.D. Lee, and H. Nagaumi: *Acta Mater.*, 2006, vol. 54, pp. 5185–94.
31. J. Chen, K. Chandrashekhara, C. Mahimkar, S.N. Lekakh, and V.L. Richards: *J. Mater. Process. Technol.*, 2011, vol. 211, pp. 245–55.
32. S. Shida: *J. Jpn. Soc. Technol. Plast.*, 1969, vol. 10, pp. 610–17.
33. H.L. Yu, X.H. Liu, X.W. Li, and A. Godbole: *Metall. Mater. Trans. A*, 2014, vol. 45A, pp. 1001–09.